Lithium Intercalation into the Titanosilicate Sitinakite

Nicholas A. Milne,[†] Christopher S. Griffith,[‡] John V. Hanna,[‡] Maria Skyllas-Kazacos,[†] and Vittorio Luca*,[‡]

Centre for Electrochemistry and Mineral Processing, School of Chemical Engineering and Industrial Chemistry, University of New South Wales, Sydney, Australia 2052, and Institute for Material and Engineering Sciences, Australian Nuclear Science and Technology Organization, Lucas Heights, Australia 2234

Received October 24, 2005. Revised Manuscript Received March 24, 2006

A preliminary investigation of lithium intercalation into the microporous titanosilicate sitinakite (with nominal formula $Na_2Ti_2O_3SiO_4 \cdot 2.76H_2O$), along with its ion-exchanged (H^+ and Li^+) and niobium-doped variant, $Na_2Ti_{1.9}Nb_{0.1}O_3SiO_4 \cdot 2.76H_2O$, is reported. The sitinakite framework intercalates lithium with some degree of reversibility; however, capacity fade and a steep voltage profile are observed. Furthermore the low potential of the intercalation reactions appears to coincide with the breakdown of the electrolyte and solvent components used in this study. Ion exchange of Na^+ in the parent sitinakite framework for H^+ shows improved electrochemical performance of the titanosilicate-based electrode composition, while Li^+ exchange affords the opposite. It is postulated that the ion-exchanged Li^+ occupies sites within the sitinakite framework which are desirable for electrochemically inserted lithium, reducing electrochemical occupancy and hence capacity. Improved electrochemical performance has been realized through the heat treatment of electrodes with capacities after 20 cycles in the range 180−200 mA h g^{-1}. This capacity compares favorably with that reported for rutile at high temperature and the recently commercialized $Li_4Ti_5O_{12}$.

Introduction

As society becomes more mobile, the demand on mobile power sources will increase. The lithium ion battery, as a secondary battery with high theoretical energy density, has therefore become important in both a research and commercial context.[1] The occurrence of lithium plating during overcharge of commercial batteries does raise serious questions with regards to the safety of current cell assemblies.[2] Hence, significant effort is being directed toward the discovery of novel materials with high energy density and good cycling characteristics that are friendly to both consumer and environment.

Titanium dioxide and titanate-based materials have been of interest as insertion electrodes in lithium batteries since it was first demonstrated by Macklin and Neat[3] that rutile exhibits good insertion capacity (approximately 100 mA h g^{-1}) and cyclability at elevated temperatures. Initially this prompted the investigation of other titanate phases including the now commercialized $Li_4Ti_5O_{12}$ with a reported capacity of 150 mA h g^{-1} and cycle life greater than 4000 cycles.[4]

One of the most important properties for the next generation of Li battery electrode materials is the ability for fast lithium ion transport through the structure. This ensures that the material is fully utilized during cell cycling rather than a thin portion at the surface of the crystal, as has been cited with intercalation into rutile in the past.[5,6] Crystalline microporous ion-exchange materials are therefore of great interest as potential lithium battery electrodes as they offer open, two-, or three-dimensional porous networks that facilitate lithium diffusion, an important criterion in determining cell performance.[7]

A recent study by Patoux and Masquelier[8] into the effect of anion groups lithium intercalation in oxide materials included one nonporous, titanosilicate phase. No significant degree of lithium intercalation in this titanosilicate was demonstrated down to a potential of 1.0 V. The reason proposed for this was that the lithium already retained in the structure did not allow for the accommodation of further lithium during reduction. It is well-known that for successful lithiation a structure needs a sufficient degree of relaxation, allowing for lattice expansion without any subsequent phase change. This aspect can be predicted by the material's ability to undergo ion exchange with large cations as well as lithium.

We and others have been extremely interested in the ion-exchange behavior of a synthetic analogue of the mineral sitinakite with the formula $Na_2Ti_2O_3SiO_4 \cdot 2.76H_2O$. Origi-

* To whom corrrespondence should be addressed. E-mail: vlu@ansto.gov.au.
† University of New South Wales.
‡ Australian Nuclear Science and Technology Organization.

(1) Tarascon, J.-M.; Armand, M. *Nature* **2001**, *414*, 359.
(2) Tobishima, S.-I.; J.-I. Yamaki, J.-I. *J. Power Sources* **1999**, *81*-2, 882.
(3) Macklin, W. J.; Neat, R. J. *Solid State Ionics* **1992**, *53*−*56*, 694.
(4) Majima, M.; Ujiie, S.; Yagasaki, E.; Koyama, K.; Inazawa, S. *J. Power Sources* **2001**, *101*, 53.
(5) Koudriachova, M. V.; Harrison, N. M.; de Leeuw, S. W. *Solid State Ionics* **2003**, *157*, 35.
(6) Luetzenkirchen-Hecht, D.; Wagemaker, M.; Keil, P.; van Well, A. A.; Frahm, R. *Surf. Sci.* **2003**, *538*, 10.
(7) Raveau, B.; Cros, C.; Doumerc, J. P.; Ebert, L. B.; Herold, A.; Lagrange, P.; Setton, R.; Guerard, D.; Besenhard, J. O.; Rouxel, J. In *Inorganic Reaction and Methods*; Hagen, A. P., Ed.; VCH Publishers: New York, 1990; p 207.
(8) Patoux, S.; Masquelier, C. *Chem. Mater.* **2002**, *14*, 5057.

10.1021/cm0523337 CCC: $33.50
Published on Web 06/17/2006

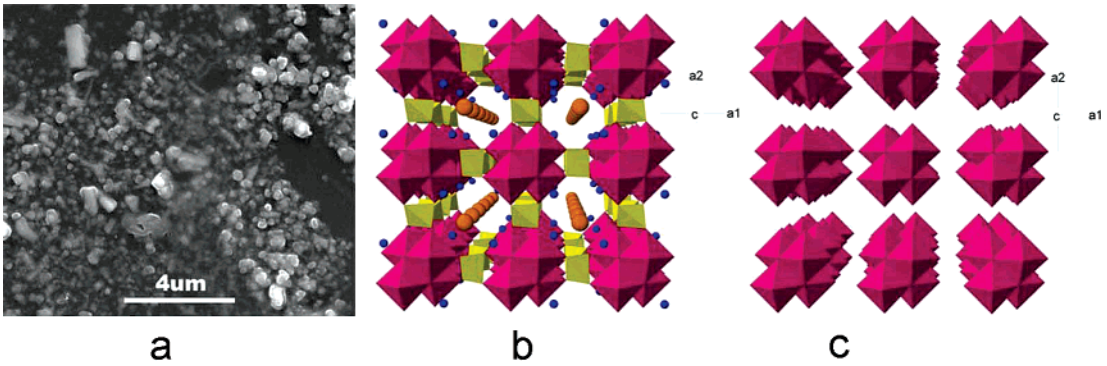

Figure 1. (a) SEM image of the parent crystalline microporous titanosilicate (sitinakite) particles, (b) structure of sitinakite ($Na_2Ti_2O_3SiO_4 \cdot 2.76H_2O$) viewed down the *c*-axis showing the connectivity of titanate wires (red) with silicate units (yellow) and alkali-metal cations (orange and green spheres) and water molecules (blue spheres) situated in the micropores, and (c) the same structure as in (b) with the exchangeable cations and silicates units removed.

nally this phase attracted significant attention from workers at Texas A&M and the U.S. DOE for its ability to absorb both radioactive cesium and strontium from alkaline radioactive waste streams. Subsequently, numerous workers have investigated this material[9−11] and its Nb-doped form.[12,13] Ostensibly, at low pH, the material possesses high selectivity for large cations, e.g. Rb^+ and Cs^+, while, at high pH, strong uptake of the smaller cations Li^+ and Na^+ occurs.[11] Extensive efforts by Clearfield and co-workers have shown that inclusion of the Cs^+ ions occurs with negligible structural change in the sitinakite framework.[9] This suggests that the material may be advantageous for intercalating lithium into the structure where lithium battery applications are considered. At the same time, the ability of the titanosilicate phase to absorb lithium indicates an ability for lithium to diffuse through the structure. It must be noted, however, that no kinetic data have so far been reported.

Sitinakite is a microporous titanosilicate mineral whose structure was first solved by Sokolova.[14] The structure of sitinakite is shown in Figure 1b and essentially consists of titania-like chains running along the *c*-axis connected by SiO_4 tetrahedra. Channels where the hydrated sodium cations reside run through the structure in the [100] direction. As part of the intense interest in this material for its potential use in radioactive waste remediation, it has been demonstrated that approximately half the sodium cations of the parent phase are exchangeable. In a lithium battery context the titanium centers should act as redox couples within the material while the silica is likely to remain inert.

What makes the sitinakite phase interesting for lithium battery applications is that the Ti:Si ratio of 2:1 is higher than other known titanosilicate phases. This means that more of the mass of the material is likely to be redox active during lithium intercalation. It can in effect be considered as an ordered assembly of titania quantum wires as is the case with ETS-10, $(Na,K)_{16}Ti_8Si_{39}O_{104}$,[15] except that the titania wires have approximately twice the cross-sectional dimensions. All of these characteristics suggested that this little studied material would make an interesting compound for investigation as a lithium ion battery electrode.

The aims of this contribution are to provide an understanding of the basic electrochemical properties of a unique titanosilicate and to investigate the effect that modifications to the structure have on these properties. One avenue for modification is through heteroelement doping of the titania wires. Doping in lithium battery electrodes is used normally to improve the electrochemical performance of a material during intercalation. Traditionally this is seen to occur through slight variations in the structure of the material, although this is probably not an issue here due to the openness of the structure. Of greater importance to this study is the ability to modify the electrochemical potential of a material using doping due to its slightly altered electronic configuration. This is one way in which the sitinakite material can be engineered for greater energy extraction in the cell. Doping the material with niobium(V) has therefore also been considered in this study.

Experimental Section

The synthesis of sitinakites was carried out using the method of Poojary and co-workers[10] with some relatively minor variations. A Ti−peroxo solution was first made by adding 47.0 mL of $TiCl_4$ to 235.0 mL of milli-Q water and 285.6 mL of 30% H_2O_2. After reaction, the final Ti concentration of the blood-red solution was 0.000 730 mol g^{-1}. A typical synthesis of sitinakite involved the dissolution of 1.876 g of Si-gel ($SiO_2 \cdot 0.69H_2O$) made by hydrolysis of tetramethyl orthosilicate (TMOS) in 60 mL of water to which 14.8 g of NaOH had been dissolved. To this solution was added 70.0 g of the Ti−peroxo solution with vigorous stirring. After standing overnight, the gel was loaded into a Teflon-lined autoclave and heated at 200 °C for 5−10 days. The white solid resulting from the hydrothermal treatment was filtered out and washed with large quantities of water in an attempt to wash away excess sodium. Nb-substituted sitinakites with general formula $Na_2Ti_{2-x}Nb_xO_3SiO_4 \cdot 2.76H_2O$ were synthesized by adding a calculated amount of Nb(V)−ethoxide (Aldrich) dissolved in 5 mL of ethanol to the Ti−peroxo solution. The amount of Nb−ethoxide added was calculated by assuming that Nb stoichiometrically replaces Ti in the ideal formula.

(9) Poojary, D. M.; Cahill, R. A.; Clearfield, A. *Chem. Mater.* **1994**, *6*, 2364.
(10) Poojary, D. M.; Bortun, A. I.; Bortun, L. N.; Clearfield, A. *Inorg. Chem.* **1996**, *35*, 6131.
(11) Clearfield, A.; Bortun, L. N.; Bortun, A. I. *React. Funct. Polym.* **2000**, *43*, 85.
(12) Luca, V.; Hanna, J. V.; Smith, M. E.; James, M.; Mitchell, D. R. G.; Bartlett, J. R. *Microporous Mesoporous Mater.* **2002**, *55*, 1.
(13) Tripathi, A.; Medvedev, D. G.; Clearfield, A. *J. Solid State Chem.* **2003**, *175*, 72.
(14) Sokolova, E. V.; Rastsvetaeva, R. K.; Andrianov, V. I.; Egorov-Tismenko, Y. K.; Men'shikova, Y. P *Sov. Phys. Dokl.* **1989**, *34*, 583.
(15) Su, Y.; Balmer, M. L.; Bunker, B. C. *J. Phys Chem. B* **2000**, *104*, 8160.

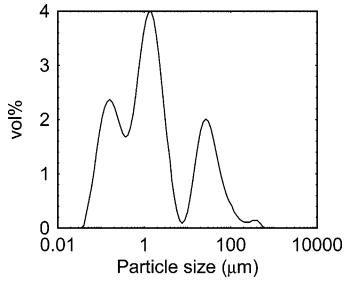

Figure 2. Particle size distribution for as-prepared sitinakite.

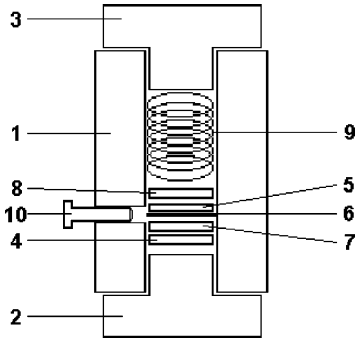

Figure 3. Schematic for a three-electrode Teflon test cell: 1, Teflon casing; 2, positive brass plunger; 3, negative brass plunger; 4, copper current collector; 5, working electrode; 6, Celgard 2500; 7, lithium ribbon counter electrode; 8, stainless steel current collector; 9, stainless steel spring; 10, stainless steel screw tipped with lithium reference electrode. In a galvanostatic cycling cell this is not included.

The as-prepared sitinakite contained 15.0 wt % water, as determined by thermogravimetric analysis using a Setaram (France) unit and exhibited a BET surface area of 47 $m^2\ g^{-1}$, measured using a ASAP2010 N_2 porosimeter. The particle size distribution was determined using a Malvern Mastersizer 2000 laser diffraction particle sizer and is shown in Figure 2.

Electrodes were prepared by a paste method where the active material, sitinakite (AM), was mixed with carbon black (Supraconductor Black XE2, Degussa, CB) to enhance conductivity and a 5 wt % solution of the binder, poly(vinylidene fluoride) (PVdF, Lexel), in *N*-methylpyrrolidinone (NMP, Sigma) to give a dry composition 80:10:10 (AM:CB:PVdF). The paste was applied to a 10 mm diameter circular disk of copper. These electrodes were dried under vacuum at 100 °C overnight (giving a typical mass between 1 and 5 mg) and then assembled as cathodes in Teflon cells, shown in Figure 3, in an argon-filled glovebox. The cells used lithium ribbon (Aldrich) as the anode, a Celgard 2500 separator soaked in Merck Battery Electrolyte LP30 (1 M lithium hexafluorophosphate in ethylene carbonate/dimethyl carbonate, 1:1 mix by weight). It should be noted that although these materials are being evaluated as potential anodes for lithium ion batteries, they are routinely tested as cathodes against the Li metal anode so as to minimize interference effects from other counter electrode materials.

Charge−discharge behavior was monitored using the Repower (China) battery testing apparatus in galvanostatic mode. Both charge and discharge current densities for these tests were maintained at 20 mA g^{-1} or C/4 (that is, one lithium/formula unit in 4 h) throughout the study. All other electrochemical measurements were performed using a Solartron (United Kingdom) Electrochemical Interface SI1287 equipped with a Solartron Frequency Response Analyzer 1255B.

Cyclic voltammetry was performed both in a three-electrode cell based on the Teflon cell design shown in Figure 3 and a more traditional three-electrode cell using a titanium counter electrode and aqueous mercury/mercurous sulfate reference electrode. Cyclic voltammetric scans were obtained by scanning in an initially negative direction from a starting potential of approximately 2.75 V vs Li^+/Li. Unless otherwise stated, the scan rate was 10 mV s^{-1}. The potentiostatic intermittent titration technique (PITT) used applied potentiostatic steps every 50 mV until the current dropped below 100 nA.

Chemical lithiation to give a sitinakite sample saturated with lithium was performed by the addition of excess *n*-butyllithium (1.6 M in hexanes, Aldrich) to a stirred slurry of the sitinakite phase in dry, degassed *n*-hexanes under a nitrogen atmosphere and ambient temperature using standard Schlenk techniques. The reaction mixture was stirred for 24 h and washed with dry, degassed *n*-hexanes before removal of the supernatant by drying under vacuum overnight. In the case of fractional reduction the slurry was cooled to −65 °C in a dry ice−acetone bath and the *n*-butyllithium added dropwise. The reaction mixture was allowed to warm to ambient temperature over 2 h and then stirred for a further 12 h before removal of the supernatant and drying under vacuum.

Capillary powder X-ray diffraction patterns of the parent titanosilicate $Na_2Ti_2O_3SiO_4 \cdot 2.76H_2O$ and Li-intercalated phases (both chemical and electrochemical) were collected on a Panalytical X′Pert Pro diffractometer (Deber-Sherrer configuration) in the range 9−65° (2θ) employing monochromatic, collimated Cu Kα radiation (1.542 Å) from a hybrid, double-bounce monochromator and a real-time multiple strip detector. All measurements were conducted on powdered samples in 0.3 mm glass capillaries (Glas, Germany) which had been sealed under vacuum. Acquired data was externally referenced to a NIST LaB_6 standard of similar capillary diameter.

^6Li and ^7Li magic-angle-spinning (MAS) and static NMR spectra were recorded at ambient temperatures on a Bruker MSL-400 spectrometer (B_0 = 9.40 T) operating at the ^6Li and ^7Li Larmor frequencies of 58.90 and 155.45 MHz, respectively. For all ^7Li measurements, a nonselective $\pi/2$ pulse length of 3 μs was calibrated on a 1.0 M LiCl solution, from which selective 0.6 μs pulses were implemented in single pulse (Bloch decay) experiments. Typical relaxation delays of 5−30 s were used for data acquisition; however, delays of up to 120 s were implemented to check for abnormally long T_1 behavior. All MAS experiments were undertaken using a Bruker 4 mm double-air-bearing probe which enabled MAS frequencies of up to 10 kHz to be achieved. ^7Li chemical shifts were externally referenced against this 1.0 M LiCl solution resonance which was set to 0.0 ppm. ^7Li static experiments were acquired with the $\theta-\tau-\theta-\tau$ solid echo experiment which used an extended 16-step phase cycle.[16] For all ^6Li MAS measurements, a $\pi/2$ pulse length of 3 μs was calibrated on a 1.0 M LiCl solution, with 0.6 μs pulses and MAS frequencies of 10 kHz being implemented in single pulse (Bloch decay) measurements.

The acquisition of MAS and static data from the air-sensitive lithium intercalation samples was aided with the use of airtight Vespel 4 mm rotor inserts manufactured by PSK Ceramics, Mulheim DE, Germany. These were loaded in an MBraun argon-filled glovebox. Dehydration of the lithium exchanged sitinakite sample was conducted at 250 °C for 5 h in a standard muffle furnace and then transferred immediately to the vacuum port and pumped on for a further 2 h before loading into a standard 4 mm zirconia rotor.

Results and Discussion

Cyclic Voltammetry. Initial chemical lithiation of the parent sitinakite phase with *n*-butyllithium showed a color

(16) Kunwar, A. C.; Turner, G. L.; Oldfield, E. *J. Magn. Reson.* **1986**, *69*, 124.

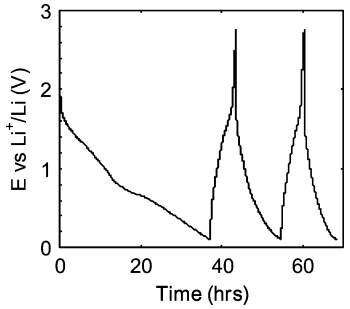

Figure 4. Typical first discharge and two subsequent cycles for the parent sitinakite material ($Na_2Ti_2O_3SiO_4 \cdot 2.76H_2O$) using a current density of 20 mA g^{-1} or a rate of C/4 (that is, 1 lithium/formula unit in 4 h).

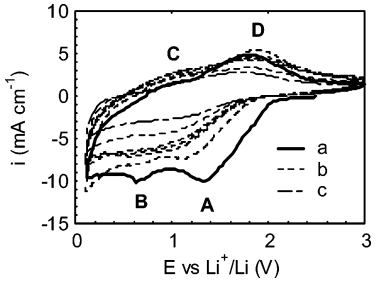

Figure 5. (a) First, (b) second, fourth, sixth, eighth, and tenth, and (c) fiftieth cyclic voltammograms for the parent sitinakite ($Na_2Ti_2O_3SiO_4 \cdot 2.76H_2O$) using a scan rate of 10 mV s^{-1} and switching potentials of 0.1 and 3 V.

transition from white to blue indicating a degree of Li intercalation to an electrochemical equivalent in the range 1.0−1.4 V vs Li^+/ Li.[17] This was confirmed by galvanostatic discharge tests (representing the intercalation reaction) of the sitinakite within a cell using a 20 mA g^{-1} current density. Capacity to 1.0 V was in the order of 275 mA h g^{-1} on the first discharge and represents a Li:Ti ratio of approximately 1.7 (assuming all of the charge transferred goes toward Li intercalation). This ratio is far too large and would suggest the formation of and then further reduction of Ti^{III} which is unlikely to be occurring. It is probable that other electrochemical reactions are occurring giving rise to higher apparent capacity. Further discharge to 0.1 V demonstrated the presence of further reduction processes; however, this region is typically not investigated for titanate materials due to the occurrence of solvent breakdown below 1.0 V. However, for reasons explained later, it has become an integral part of this study.

Figure 4 shows a typical voltage response for the first three galvanostatic cycles for sitinakite between the potentials 0.1 and 2.75 V. This highlights significant capacity in the region of 600−800 mA h g^{-1} on the initial discharge. However, this capacity value is not constant decreasing to 80 mA h g^{-1} within 20 cycles. This capacity fade is believed to be due, at least in part, to the occurrence of solvent breakdown.

Figure 5 shows the first, tenth, and fiftieth consecutive cyclic voltammograms for sitinakite using scan rates of 10 mV s^{-1}. The first cycle shows the occurrence of two reduction peaks—one at approximately 1.35 V (peak A) and the other at approximately 0.65 V (peak B). Both appear to reach approximately the same peak current, assuming their background currents are similar. The appearance of a peak in cyclic voltammetry generally occurs through the depletion of active material at the electrode surface due to limits in diffusion. The higher potential reduction peak, A, is therefore attributed to the intercalation of lithium into the structure, as was indicated by the ability to chemically lithiate with *n*-butyllithium. The reverse reaction for this reduction has been ascribed to the oxidation peak D at approximately 1.8 V. This feature shows a large degree of reversibility for this reaction. The other reduction peak, B, occurs in the region typically avoided due to solvent and electrolyte degradation. The peak itself, however, is unlikely to represent solvent degradation. During solvent reduction no diffusion limit to the reaction would be reached (molecules are always present at the electrode's surface). As such solvent reduction is represented as a region of increasing current unless a species in equilibrium with the main constituents is involved. This leaves the possibility of either a reaction involving the hexafluorophosphate component of the electrolyte or of further lithium intercalation. It should also be noted that the reverse of this reaction, labeled C in Figure 5 and occurring at approximately 1.0 V vs Li^+/Li, is of quite low current. This suggests that the mechanism at play involves another irreversible reaction or decomposition of the product formed at peak B and supports the possibility that this reaction couple could be attributed to electrolyte interference.

Investigations aimed at confirming the possible interference of electrolyte decomposition were undertaken using cyclic voltammetry on the parent sitinakite electrodes and their substrates using $LiPF_6$ and tetrabutylammonium hexafluorophosphate (Bu_4NPF_6) solutions. In the Bu_4NPF_6 solution a significant increasing current was observed below approximately 1.1 V vs Li^+/Li that would be representative of solvent decomposition. For reduction in the range 0.1−3.0 V, however, no distinct peaks were observed. Interestingly, on the native copper substrate a cathodic peak was observed in the range 1.9−2.0 V vs Li^+/Li in $LiPF_6$ that was not apparent in Bu_4NPF_6. This has been attributed previously to the reduction of PF_6^--related species particularly in the presence of moisture.[18] These reactions are hypothesized to be responsible for the fouling of copper that consequently suppresses solvent decomposition on this surface.[19] It seems plausible that the weak shoulder observed on peak A at approximately 2.0 V in Figure 5 is a result of this electrolyte reduction. Though this peak is not present for sitinakite in the Bu_4NPF_6, it does not appear under the same conditions for copper either and appears to be dependent on the presence of lithium ions in the electrolyte. This raises the possibility of suppression of the solvent decomposition reactions on the sitinakite surface in a manner similar to that observed with copper. However, from the shape of the subsequent voltammograms, with the increasing background current below 1.1 V, it is reasonable to assume that degradation occurs at least to some extent. What is ultimately apparent though is

(17) Whittingham, M. S.; Dines, M. B. *J. Electrochem. Soc.* **1977**, *124*, 9, 1387.

(18) Aurbach, D.; Zaban, A. *J. Electroanal. Chem.* **1995**, *393*, 43.

(19) Guidotti, R. A.; Nelson, G. C. In *Materials for Electrochemical Energy Storage and Conversion II-Batteries, Capacitors and Fuel Cells*; MRS Symposium Proceedings 496; Ginley, D. S., Doughty, D. H., Scrosati, B., Takamura, T., Zhang, Z., Eds.; MRS: Warrendale, PA, 1998; p 469.

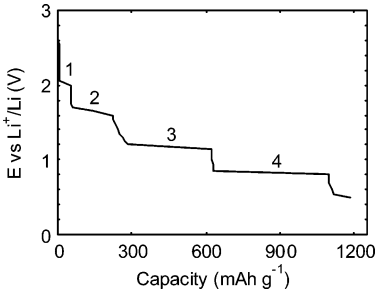

Figure 6. Thermodynamic results of the potentiostatic intermittent titration technique on the parent sitinakite showing four energy levels. If all four levels contributed to lithiation, this would give a final composition of $Li_{11.5}Na_2Ti_2O_3SiO_4$. Even after consideration of the effects of nonintercalation events, the capacity is improbably high and it is stressed that the plot only provides a qualitative model of the system.

that electrolyte and solvent effects are not likely to be attributable to peak B. Intercalation, therefore, becomes the most probable source.

Potentiostatic Intermittent Titration. Investigation of the sitinakite electrode material by a preliminary potentiostatic intermittent titration technique (PITT) shown in Figure 6 revealed four discrete energy levels at approximately 2.0, 1.6, 1.1, and 0.77 V. It must be noted that these plateaus are not visible in the discharge plot as this is not necessarily under equilibrium conditions, while the thermodynamic plot from the PITT experiment is performed under conditions where equilibrium is achieved at each step. The capacity for sitinakite determined from this plot is in the order of 1120 mA h g^{-1}. It is possible to calculate a final composition of $Li_{13.8}Na_2Ti_2O_3SiO_4 \cdot 2.76H_2O$ (although the water is unlikely to be in this form at this point and will be dropped from further discussion). This gives a lithium-to-titanium ratio of almost 7 and is highly improbable (a maximum ratio of 4 would be expected from the full reduction of titanium centers from Ti^{IV} to Ti^0). As such some of the energy levels shown must in fact result from reactions other than intercalation making an assignation of the plateaus imperative. The first energy level in the PITT (plateau 1) probably corresponds to the shoulder on peak A in the cyclic voltammograms presented in Figure 5. The region at 1.6 V (plateau 2) is almost certainly the couple A/D in the cyclic voltammetry shown in Figure 5, lying approximately halfway between the two in potentials. We believe that this energy level therefore represents genuine lithium intercalation. If this analysis is correct, a lithium-to-titanium ratio slightly greater than 1 can be calculated. This is somewhat higher than what was expected from chemical lithiation, in which a one-to-one ratio was not achievable. It also represents the reduction of all Ti^{IV} in the sitinakite to Ti^{III}. Though this is plausible, there are still two plateaus (3 and 4) below this one, potentially associated with intercalation. This would imply an ability to further reduce Ti^{III} in the structure. This is a possibility with the Ti^{II} redox state potentially accessible. Further reduction to the Ti^0 redox state may even be possible as has been seen by Poizot and co-workers.[20] These investigators have found that the reduction of MO (where M is Co, Ni, Cu, Fe) to the zero redox state is possible for nanocrystalline materials. If the TiO_6 nanowires in the original structure are viewed as discrete quantum systems, a similar change in the accessibility of lower redox states for Ti may be possible. However, such a drastic change in redox behavior appears unlikely and some interferences must be assumed. Part of the overestimate of capacity comes about through the effect of residual current on the PITT experiment, particularly with the low 100 nA termination step. If this effect is significant enough, an overestimate of the capacities would be expected. Consequently, we believe that the data obtained through this experiment are only of use qualitatively and quantitative interpretation should be approached with caution.

The remaining two plateaus (3 and 4) of the PITT energy plot are likely to have contributed to peak B in the voltammograms. It is safe to assume that one of these is due to intercalation as the peak is not present in a non-lithium electrolyte; the other is likely to be associated with reduction of the solvent. In a comparison of these potentials to those of the B/C peak couple in Figure 5, it seems most likely that the 0.77 V plateau (4) is associated with these peaks and therefore intercalation. It is important to note that the flat appearance of plateau 4 very strongly suggests a two-phase intercalation mechanism. The other plateau at 1.1 V (plateau 3) occurs at a potential comparable to that for the onset of solvent decomposition in non-lithium electrolyte and, as such, has been ascribed to this phenomenon. As stated earlier, a quantitative interpretation of the capacity data should be approached with caution. Analysis of the 0.77 V plateau (plateau 4) suggests an ultimate Li:Ti ratio greater than 4. However, with solvent reduction already predicted to be occurring in the system, significant side reactions and capacity overestimation for this plateau can be assumed. Therefore, the actual degree of intercalation, or reduction, at this point cannot be accurately determined.

Ultimately, our analysis of the PITT data highlights that at least two energy levels are associated with lithium intercalation, and this raises the possibility of two different intercalation sites for lithium. For the sodium form of sitinakite, Poojary and co-workers[10] have identified two unique sodium exchange sites. One 4-fold site is positioned at 0, 0.5, 0.5, with the second site (site 2′) located at approximately 0.435, 0.435, 0.06. It is only the second of these sodium sites that can be exchanged from aqueous solution. It is possible that a similar scenario also applies to Li intercalation; that is, it can be inserted into two possible sites but cannot be extracted from one. This supports the appearance of only one reversible peak in the cyclic voltammograms.

Of greater importance are the subsequent voltammograms shown in Figure 5. After a number scans, the lower potential peak, B, decreases in current with only one clear peak, A, remaining visible after 10 scans. This peak decreases in potential over the cycling to eventually drop below 1.0 V—the lower potential limit that is normally used for titanates. To account for this and the suspected 0.77 V intercalation plateau observed in the PITT experiments (Figure 6), galvanostatic cycling experiments were performed with upper and lower switching potentials of 2.75 and 0.1 V versus $Li^+/$

(20) Poizot, P.; Laulelle, S.; Grugeon, S.; Dupont, L.; Tarascon, J.-M., *Nature* **2000**, *407*, 496.

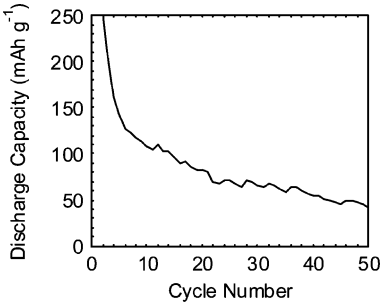

Figure 7. Typical discharge capacity plot for sitinakite over 50 cycles using a galvanostatic charge/discharge regime. The current density was 20 mA g^{-1} and switching potentials were 0.1 and 2.75 V. The initial discharge capacity for the cell shown was approximately 750 mA h g^{-1}.

Li, respectively. A discharge capacity plot of the parent sitinakite is shown in Figure 7 and demonstrates a significant difference between the first discharge and subsequent discharge capacities. This is to be expected due to the rapid degradation of the lower potential reaction (B/C) in the cyclic voltammograms (Figure 5). However, a degree of capacity fade remains throughout the plot. After 20 cycles the typical discharge capacity is 80 mA h g^{-1}, and this is halved after 50 cycles. This could be explained by four possible mechanisms: (1) structural change of the sitinakite framework; (2) poor diffusion characteristics through the structure; (3) strong lithium binding at intercalation sites resulting in poor reversibility; (4) interference on the surface of the material, for example a film, from solvent or electrolyte reduction preventing intercalation reactions.

One possible source of structural change in sitinakite in a lithium battery comes from the effect of HF that is always present in $LiPF_6$-based electrolytes. The action of HF on the sitinakite electrode might be expected to result in the SiF_6^{2-} species. To investigate this possibility, sitinakite was contacted with an excess of electrolyte for 1 month and the structure subsequently examined by XRD. These investigations showed no change to the sitinakite structure, and we believe that significant chemical degradation by HF in the electrolyte is unlikely to occur over the medium term. However, electrochemically induced structural changes represent another possibility.

X-ray Diffraction. To investigate the response of the sitinakite structure during cycling, XRD patterns were recorded in sealed capillaries of materials that had been electrochemically lithiated to a potential of 0.1 V using steadily decreasing currents in a powder cell based on the design of Jiang and Dahn.[21] Figure 8 shows the XRD patterns of sitinakite materials reacted in various ways. It is apparent that there is some variation in the position of the main 100 reflection of sitinakite centered at about 11° in 2θ. First, it is possible to discern that on drying (Figure 8b), a small lattice contraction occurs relative to the as-prepared material (Figure 8a) as is expected for removal of water associated with hydration of exchangeable cations within the channels of zeolitic materials.[22] In a comparison of the patterns of

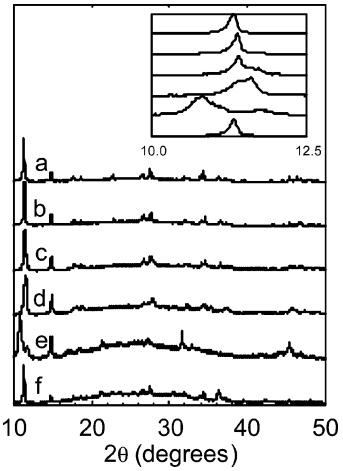

Figure 8. XRD patterns for the (a) parent sitinakite, before lithiation ($Na_2Ti_2O_3SiO_4 \cdot 2.76H_2O$), (b) parent sitinakite dried at 200 °C ($Na_2Ti_2O_3SiO_4$), (c) partially chemically reduced sitinakite with a Li:Ti ratio of 0.25 ($Li_{0.5}Na_2Ti_2O_3SiO_4$), (d) saturated chemically lithiated sample, (e) the electrode material after a single discharge, and (f) after 50 cycles and reoxidation over the range 10−50° in 2θ and (inset) 10−12.5° in 2θ.

the as-prepared (Figure 8a) and dried sitinakite (Figure 8b) with those of the two chemically lithiated dehydrated sitinakite samples (Figure 8c,d), two independent sitinakite 100 reflections can be noted. These data show unequivocally that two types of structurally similar sitinakites are generated on Li insertion that differ in their unit cell dimensions. One of these reflections occurs at the same angle as for the dehydrated sample whereas the other reflection occurs at higher angle representing an even more contracted lattice. It seems clear that this contracted phase is generated by movement of Li into the sitinakite channels to occupy discrete lattice sites and possibly also further reduction of some of the titanium centers. However, the quality of the present laboratory X-ray data precludes meaningful Rietveld analysis and high-quality synchrotron X-ray data, neutron data, or preferably both would be desirable to determine the lithium siting with any precision.

When Li is inserted by electrochemical means, the results are quite different. There is a large shift in the main reflection to lower angles relative to both the dehydrated sample and the chemically lithiated samples indicating a very significant expansion of the unit cell. At the same time a small quantity of the more contracted phase persists. Again there is no evidence to suggest structural collapse under the conditions used only relatively significant changes unit cell dimension. It would seem that this expansion of the lattice on deeper lithium insertion is due to reduction of Ti^{III} and the filling of sites other than those responsible for the initial contraction. The large channels of the framework would allow for this expansion while not necessarily inhibiting further intercalation. That such changes in lattice dimensions can occur when cations migrate in zeolitic materials is well established. The fact that some contracted phase remains even after "full" intercalation indicates that the lithium insertion reaction does not proceed to completion in the sample as a whole or in all individual crystallites. This deeper electrochemically driven lithium insertion and filling of secondary sites in the structure is probably associated with the 0.77 V plateau in the PITT

(21) Jiang, J.; Dahn, J. R. *Electrochem. Commun.* **2004**, *6*, 724.
(22) Johnson, M.; O'Connor, D.; Barnes, P.; Catlow, C. R. A.; Owens, S. L.; Sankar, G.; Bell, R.; Teat, S. J.; Stephenson, R. *J. Phys. Chem. B* **2003**, *107*, 942.

data of Figure 6, significantly below the standard titanate discharge potential of 1.0 V vs Li^+/Li.

Reoxidation of the sitinakite subjected to 50 cycles by exposure of the electrode material to air completely restores the pattern such that it is qualitatively the same as the pattern of the dehydrated sample (Figure 8f). It should be reiterated that the XRD patterns of Figure 8e,f are from actual electrode materials and include carbon black and PVdF and can therefore only provide a qualitative indication of the structure of the titanosilicate component. Nonetheless, these data prove that the sitinakite material is stable under cycling and that changes in cell dimension and disorder are attributable to lithium insertion and occupation of at least two distinct structural sites. The broadening of the peaks of the parent material on lithium insertion (compare Figure 8a to Figure 8c,d,e) indicates that the intercalation reaction generates considerable disorder in the system which is reversible like the changes in unit cell dimensions. Broadening of X-ray reflections may indicate an increase in lattice strain and/or a reduction in the scattering domain size. However, with shallow intercalation giving predominantly the contracted phase and deeper intercalation the expanded phase within a single particle, then domain size shrinkage and broadening would also result in direct analogy to what has been observed on lithium intercalation in anatase.[23,24]

Though lattice strain can be assumed due to the large changes in lattice parameters as stated earlier, they appear to be reversible. In a comparison of Figure 8b to Figure 8f, there is very little evidence of broadening (only a very small difference in line width is observed). It is possible for strain in the lattice to result in electrochemical grinding[25] that ultimately results in the cracking of particles and increases resistances in the system over cycling. Ultimately this means that the cell capacity will fade as resistance effects push the cycling reaction potentials outside the operating window. However, a lack of broadening suggests this was not significant over 50 cycles and the changes in lattice parameter may not have been significant enough to cause this effect. Further quantification of variation in lattice parameters is planned as a measure of this effect.

^{6}Li and ^{7}Li Solid-State NMR. Both static and MAS NMR spectroscopy was used to probe the local lithium environments within the reduced sitinakite structure. The ^{6}Li ($I = 1$) nucleus is an attractive NMR nucleus as it is approximately 7.5% naturally abundant and possesses very small quadrupole and magnetic dipole moments in comparison to ^{7}Li. As a result, under typical MAS experimental conditions the ^{6}Li−^{6}Li dipole−dipole couplings are easily averaged out, and well-resolved resonances with narrow line widths are generally observed even at very modest lithium concentrations. The ^{7}Li nucleus offers a useful complement to solid-state ^{6}Li studies that have been undertaken to maximize chemical shift resolution. While the central (+1/2 to −1/2) transition of this $I = 3/2$ nucleus does not render the chemical shift resolution afforded by its ^{6}Li counterpart, the quadrupolar parameters and line shape characteristics exhibited by the (±3/2 to ±1/2) satellite transitions do offer insights into structural aspects of the systems under study.

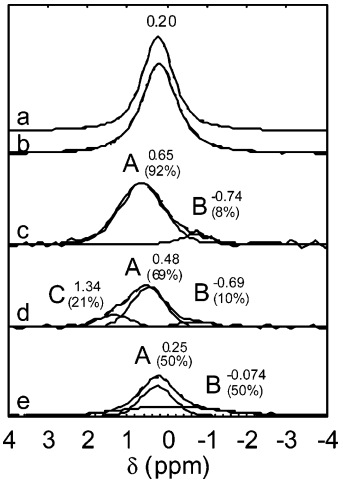

Figure 9. Deconvolution of ^{6}Li MAS NMR spectra for (a) a Li^+-exchanged sitinakite, (b) a Li^+-exchanged sitinakite after vacuum-drying, (c) partially chemically reduced sitinakite with Li:Ti ratio of 0.25 ($Li_{0.5}Na_2Ti_2O_3SiO_4$), (d) saturated chemically lithiated sample, and (e) a sitinakite electrode reduced electrochemically.

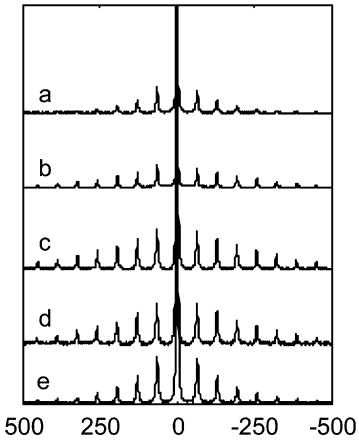

Figure 10. ^{7}Li MAS NMR spectra for (a) a Li^+-exchanged sitinakite, (b) Li^+-exchanged sitinakite after vacuum-drying, (c) partially chemically reduced sitinakite with Li:Ti ratio of 0.25 ($Li_{0.5}Na_2Ti_2O_3SiO_4$), (d) saturated chemically lithiated sample, and (e) a sitinakite electrode reduced electrochemically.

Figures 9−11 show the ^{6}Li MAS NMR data and the ^{7}Li MAS and ^{7}Li static NMR data, respectively, for a series of Li-intercalated sitinakite samples. The ^{6}Li MAS NMR spectrum (see Figure 9a) of the Li^+-exchanged sitinakite material displays a single resonance at 0.2 ppm that can be satisfactorily simulated using a single peak which is predominantly a Lorentzian function. Dehydration of this sample results in only a minor downfield shift of the ^{6}Li resonance to 0.22 ppm and similar line width and Gaussian/Lorentzian ratio. It is interesting to note that the satellite transition line shapes from the ^{7}Li MAS and static studies of Figures 10a,b and 11a,b do not exhibit any significant quadrupolar structure, and this is probably attributable to a lack of short-range order in these sites. This suggests that the lithium incorporation into the sitinakite structure by an ion exchange route is characterized by some degree of disorder associated with the lithium positioning within the cavity structure, as was

(23) Luca, V.; Hanley, T. L.; Roberts, N. K.; Howe, R. F. *Chem. Mater.* **1999**, *11*, 2089.
(24) Wagemaker, M.; Kearley, G. J.; van Well, A. A.; Mutka, H.; Mulder, F. M. *J. Am. Chem. Soc.* **2003**, *125*, 840.
(25) Ohzuku, T.; Ueda, A. *Solid State Ionics* **1994**, *69*, 201.

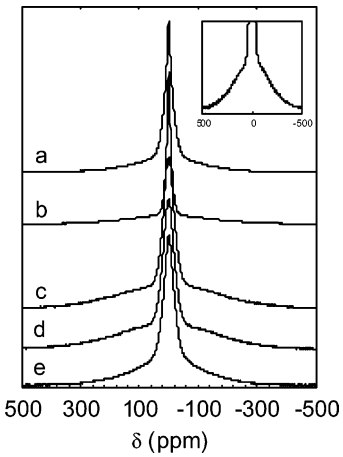

Figure 11. Static ^{7}Li NMR spectra for (a) a Li^{+}-exchanged sitinakite, (b) a Li^{+}-exchanged sitinakite after vacuum-drying, (c) partially chemically reduced sitinakite with Li:Ti ratio of 0.25 ($Li_{0.5}Na_2Ti_2O_3SiO_4$), (d) saturated chemically lithiated sample, and (e) a sitinakite electrode reduced electrochemically.

previously seen by Poojary and co-workers during their structural investigations of the sitinakite phase.[10] A significantly broader satellite transition spectrum is observed for the dehydrated sample in comparison to its hydrated analogue, implying that intercalated water directly influences the lithium speciation and solvation within these channels.

The ^{6}Li MAS spectra of samples that were prepared by *n*-butyllithium (Figure 9c,d) reduction are significantly broadened in comparison to the ion-exchanged phases, and the main resonance appears at lower field. This broadening could also be associated with shrinking domain size as was suggested from the XRD data. Spectral decomposition of the partially inserted sample can be best achieved with a minimum of two species (A and B) at 0.65 (92%) and −0.074 ppm (8%), while at higher insertion (Figure 9d) an additional feature (species C) is required at 1.34 ppm. The existence of multiple Li species is consistent with the XRD and PITT data that show multiple intercalation events. It is interesting to note that on increased insertion the species A and B resonance move to higher field indicating a decreased shielding at the ^{6}Li nuclei relative to the less intercalated sample. The appearance of species C which accounts for about 21% of the total intensity is difficult to explain but is clearly due to Li in quite a different environment in which the shielding is higher.

The existence of discrete intercalate phases has been ascertained by XRD and can also be inferred from the PITT experiments. The appearance of the two minor resonances may simply be a product of new lithium sites within the same phase or to lithium sites in the two different intercalated phases. It is interesting that the second resonance only appears in the chemically saturated sample and that this would not necessarily support the data obtained from XRD or PITT as it suggests a new site has been accessed between the low level intercalated sample and the saturated sample. However, it should be noted that inclusion of a species C resonance to the partially inserted sample (Figure 9c) could not be justified with the current data quality. We have been unable to obtain a spectrum with higher signal-to-noise that can definitively confirm the existence of this species for this material. Thus, within the limitations of the present data one must surmise that the spectra of the chemically inserted samples are obtensibly the same.

Spectral decomposition of the ^{6}Li MAS NMR spectrum of the electrochemically intercalated sample (Figure 9e) reveals a species A resonance centered at 0.25 ppm (∼50%) with a further component B at −0.074 ppm (∼50%). The species A resonance continues its progressive shift to higher field compared to the partially chemically intercalated and saturated samples. This shift to higher field of species A may be due to an increase in the state of reduction of the sample since electrochemical reduction should insert more lithium and generate a larger proportion of reduced titanium centers. Possible sources of interference have been eliminated through the thorough washing of the electrode with dimethyl carbonate, which ensures the removal of all soluble lithium hexafluorophosphate species. It is also worth considering however that any interactions between the carbon conductivity enhancer and lithium have not been taken into account.

The small chemical shift range of ^{6}Li makes this nucleus extremely sensitive to changes in the chemical and electronic environment about the ^{6}Li nuclear spin. Past work by Xu and co-workers[26] has demonstrated that changes in chemical shift of the observed ^{6}Li resonance can be attributed to changes in the coordination number about the lithium nuclei. Lower coordination number leads to increased shielding and lower chemical shifts, with higher coordination numbers leading to high field and chemical shift.

In the absence of further localized structure information about the lithium environment in the chemically reduced samples it appears reasonable to infer that coordination numbers of either 3 or 4 prevail during the initial stages of sitinakite reduction while in the electrochemical case there is cursory evidence that coordination numbers >4 about lithium are present in the reduced phase. The electrostatic forces subjected to the lithium ions by this "crowding" could easily reasonably explain the expansion of the lattice parameter seen in the XRD.

The satellite transition line shapes of the ^{7}Li MAS and ^{7}Li static NMR for the reduced samples (Figures 10c,d,e and 11c,d,e) seem to provide some further support of the XRD data in terms of disorder. The two chemically reduced samples show a degree of quadrupolar behavior that is particularly evident in the static spectra. Though very minor, this quadrupolar behavior does suggest at least a degree of short-range order in the lithium positions. In the case of the electrochemically reduced sample there is clearly no quadrupolar nature in the line shape, suggesting there is very little order in the lithium positions. The ^{6}Li NMR data (Figure 9e) also suggest this with the very broad resonance B. As such, these data suggest that the increased lithiation has increased the degree of disorder as has been seen with anatase in the past.[23] This provides further evidence for reversible disorder that was shown by the broadening of the primary reflection in the XRD patterns (Figure 8).

Ion-Exchanged Sitinakite. The pores of the parent sitinakite structure contain hydrated sodium counterions. In

(26) Xu, Z.; Stebbins, F. *Solid State Nucl. Magn. Reson.* **1995**, *5*, 103.

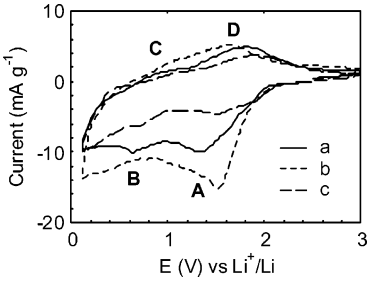

Figure 12. Cyclic voltammograms for (a) the parent sitinakite and (b) the H^+-exchanged and (c) the Li^+-exchanged sitinakites using a scan rate of 10 mV s^{-1} and switching potentials of 0.1 and 3 V. The working electrodes had a surface area of $\pi/4$ cm^2.

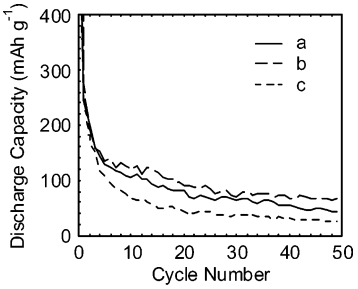

Figure 13. Plot of the discharge profiles for (a) parent sitinakite, (b) H^+-phase sitinakite, and (c) Li^+-phase sitinakite using switching potentials of 0.1 and 2.75 V and a current density of 20 mA g^{-1}.

an effort to alter the pore interactions and therefore the diffusion characteristics, the Na^+ counterions were exchanged with H^+ and Li^+ and the electrochemical characteristics of the two resultant phases compared. The cyclic voltammograms for these phases, shown in Figure 12, display characteristics different from that of the parent Na^+ phase. The H^+ phase displays only one clear reduction peak in the cyclic voltammogram with the lower potential peak, B, observed in the Na^+ phase not readily apparent. This appears to indicate that one site originally accessible to intercalated lithium in the Na^+ phase is not available in the protonated form. The reason for this remains unclear but could be due to Na^+ "directing" the intercalated lithium rather than the lithium being allowed to find its own minimum energy position. In the Li^+ phase, both reduction peaks are present; however, the shoulder on the higher potential peak, A, appears stronger. The shoulder was observed in the Na^+ phase; however, it is not particularly strong in terms of current, while in the Li^+ phase the peak current of the shoulder is significantly closer to that of the main peak.

As shown in Figure 13, cycling of the ion-exchanged sitinakites between the potentials of 0.1 and 2.75 V shows very poor results for the Li^+-exchanged sitinakite. The discharge capacity of the material is roughly half that of the Na^+ phase. The H^+ phase on the other hand shows a slight improvement in its discharge capacity. It is reasonable to surmise that in the case of the H^+ phase that the smaller cation dimension (of H^+/H_3O^+) would lead to greater ease in the movement of Li^+ ions through the structure. This would in turn lead to greater utilization of the phase and, therefore, greater capacity. In the case of lithium it is proposed that the ion-exchanged Li^+ occupies sites that would normally be accessible to intercalated lithium. This is similar to what was observed by Patoux and Masquelier

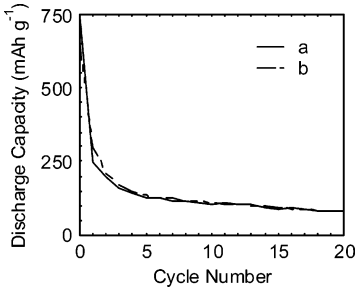

Figure 14. Plot of the discharge capacities for (a) the parent sitinakite ($Na_2Ti_2O_3SiO_4 \cdot 2.76H_2O$) and (b) the 5% Nb-doped sitinakite ($Na_2Ti_{1.9}Nb_{0.1}O_3SiO_4 \cdot 2.76H_2O$) using switching potentials of 0.1 and 2.75 V and a current density of 20 mA h g^{-1}.

for other materials.[8] This would give the Na^+-exchanged material a much larger capacity as the Na^+ ions do not occupy the same sites within the sitinakite structure as the exchanged Li^+. The cyclic voltammograms for the Li^+-exchanged sample, however, do not show one specific site being lost. The two reduction peaks and one shoulder are all present, but the different peak heights suggest a change in the diffusion coefficient for the lithium ions in each of the exchanged samples. This is obviously an issue that requires further investigation.

Framework Doped Sitinakite. Further alterations to the structure were achieved through the doping of the sitinakite framework with 5% niobium. This effect has been well investigated in the past, and it is known that up to 5% Nb can be incorporated into framework sites.[12] The doping yielded results that showed little improvement with respect to the parent material. Figure 14 gives the typical discharge capacity plots for sitinakite and the niobium-doped variant studied. After 20 cycles the doped sitinakite performs no better or worse than the undoped version. This implies that in its current form the electrochemical properties cannot be improved by this low degree of doping with niobium. It does not however rule out other transition metal dopants as possible sources of improvement, leaving open the possibility of using the dopants to alter the potential of a cell without adversely affecting the electrochemical performance, therefore providing a way to engineer the energies of the reaction more effectively.

Influence of Water. The effect of the hydrated cations situated in the micropores of the sitinakite framework has been considered for the H^+ and Li^+ ion-exchanged sitinakite phases. However, it is also important to consider the impact that the water of hydration present in these phases has upon the intercalation of lithium. The typical procedure of electrode preparation through drying under vacuum at 100 °C is unlikely to fully remove the water from the channels of the sitinakite framework. Thermogravimetric analysis, shown in Figure 15, suggests a treatment of at least 250 °C would be required to ensure complete removal of water from the micropore channels under ambient pressure (though this would of course be lower under reduced pressure). Also, the reversibility of dehydration for the sitinakite phase means that significant amounts of water may be absorbed on exposure to the atmosphere or from trace water present in the electrolyte. The resultant effects cannot be separated from

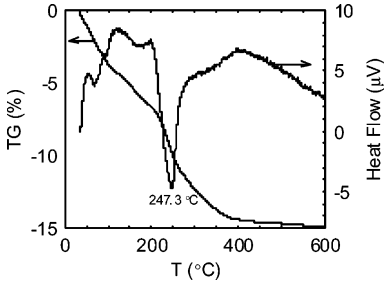

Figure 15. Thermogravimetric analysis results for the parent sitinakite sample.

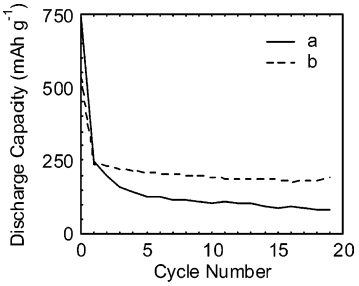

Figure 16. Discharge capacity profile for (a) undried sitinakite and (b) sitinakite dried under vacuum at 200 °C for 2 h. The switching potential were 2.75 and 0.1 V, and the current density was 20 mA g^{-1}.

an interpretation of the observed electrochemical performance.

The micropore water will have a number of potentially undesirable effects. First, its electrochemical action could result in its reduction or the reoxidation of the reduced titania nanowires within the sitinakite framework. This would mean more current on the initial discharge would go to irreversible reduction reactions, resulting in a higher initial capacity for the material than would otherwise be expected. The significant reduction in capacity between the first and subsequent discharges could easily be the result of this effect. If this were the case, removing the micropore water would reduce the initial discharge capacity to a level closer to the subsequent discharges. Also, the "precipitation" of lithium oxides and/or hydroxides within the channels is possible, presumably leading to the blockage or restriction of these channels. As a consequence, diffusion of lithium would be inhibited and the cyclability of the electrode significantly reduced. Under this interference mechanism, removing micropore water should improve later discharge capacities of the electrode but not necessarily the initial capacity. Finally, removal of micropore water would likely change the location of the cations within the channels as these ions migrate toward the walls of the channels to be stabilized by the oxygen ligands of the silica tetrahdra and titania octahedra to be found there. The result of this structural rearrangement is that the channels would become far more accessible to migrating cations with a significant increase in the diffusion, and hence, in the capacity of the large particles. The question, of course, is whether the new site of the cations within the channels would be closer to the preferred sites of intercalated lithium thereby potentially reducing the capacity of the material.

To briefly investigate this scenario, the Na^+-exchanged sitinakite electrodes were subjected to drying under vacuum at 200 °C for 2 h and the subsequent discharge profiles measured. Figure 16 shows a typical profile for the dried electrode compared to the undried parent phase. The capacity of the dried electrode material has more than doubled to about 180 mA h g^{-1} by the 20th cycle (comparing favorably with both $Li_4Ti_5O_{12}$ at 150 mA h g^{-1} and rutile at 100 mA h g^{-1}), although the large drop in capacity from the first cycle does cause problems practically with a significantly larger mass of cathodic material required to keep the cell initially balanced, while the initial discharge increased significantly. This effectively rules out the possibility of reoxidation, while the blockage of the pores seems somewhat unlikely for electrodes which are likely to contain more adsorbed water than the more rigorously dried variants. Understanding what exactly is causing the increase in capacity across the board will be the subject of a further paper.

Intercalation Model. From the data obtained, a model for intercalation can be proposed and is depicted in Figure 17. The figure shows three particles sizes as reflected in the particle populations determined from the particle size analysis in Figure 2. Stage 1 represents the low-level, or shallow, intercalation observed in the chemically lithiated samples. This appears structurally and symmetrically similar to the parent material but with a contracted unit cell. When a high-level, or deep, intercalation is provoked using electrochemical means (stage 2) an expanded phase results as more lithium is intercalated. Again the structure appears similar to the parent sitinakite phase but with a significantly expanded unit cell dimension. In both cases the smaller particles become fully intercalated to either the contracted or expanded phase in the early stages of intercalation. The larger particles however will only partially intercalate and therefore contain domains of intercalation, illustrated by the broadening observed in the XRD reflections as is seen in anatase.[23,24] This will generate strain in the crystal and if the change in lattice parameter is large enough potentially promote electrochemical grinding.[25] It is possible that the effect may even prevent the intercalation reaction from reaching completion. This would help explain why the fully loaded sitinakite sample (Figure 8e) still shows evidence of the contracted sitinakite phase.

Similarities between sitinakite and other titania-based anode materials can be drawn. As mentioned previously the separation of sitinakite into phases similar to the parent material but with different lithium content is very similar to that of anatase.[24] There are also similarities with the thin intercalated film that results from lithiation of rutile stemming from its poor diffusion properties.[5,6] The possible effects of diffusion limitations can also been seen in this system. Although the large structural channels offer the possibility of fast diffusion, it is only with the removal of water from the pores that high reversible capacities can be reached. Reduction in the size of the cations within the pores also assist in improving reversible capacity.

The NMR results demonstrate that up to 3 distinct Li sites (A−C of Figure 9) are present within the contracted phase, with species C only becoming differentiated as more Li is intercalated. Deep electrochemical intercalation results in a spectrum that superficially resembles that of the chemically

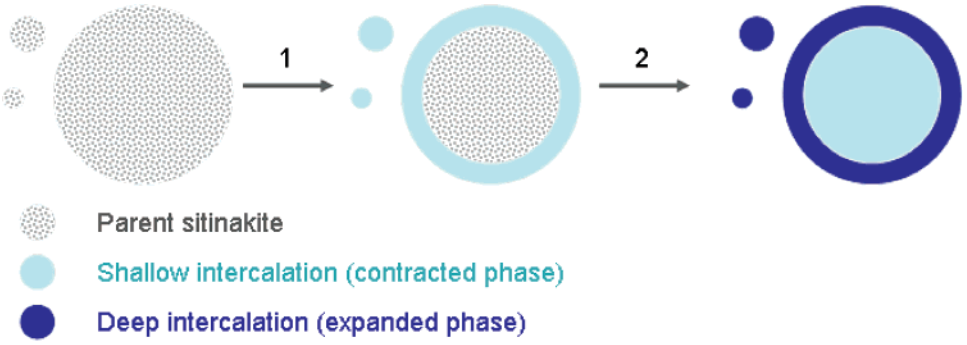

Figure 17. Depiction of the intercalation model developed for sitinakite. Three different sized particles have been used to illustrate the three main populations of particles evident in the parent sitinakite.

intercalated materials. However, what are termed the species A and B resonances in the NMR spectrum of this highly intercalated material have somewhat different line widths compared with the chemically intercalated materials. The width of the species A resonance decreases while that of the species B resonance is broadened enormously. This highlights that in terms of disorder these sites are quite distinct, and we postulate that species B now represents an envelop of sites associated with the expanded phase which also displays a very broad (100) reflection.

Conclusions

The microporous titanosilicate known as sitinakite has shown some useful intercalation capacity. By a further understanding of the mechanism of the reactions involved and modification of the basic framework in terms of composition and structure, these capacities can be potentially improved. Even for this unoptimized material, the capacity observed after the 20th cycle of around 200 mA h g^{-1} is much higher than that of $Li_4Ti_5O_{12}$ although sitinakite appears to have poorer cycling properties and a smaller voltage plateau.

The sitinakite structure appears stable under the conditions investigated with no evidence of phase changes although lattice contraction and expansion is observed on electrochemical intercalation. XRD investigation shows that several discrete intercalates are formed on lithium insertion and these may be due to differential lithium concentrations in different parts of a single particle. Solid-state lithium NMR highlights the multiplicity of the lithium site occupancy and the disorder associated with intercalation. The results are therefore reminiscent of lithium intercalation in anatase, which has now been extensively studied.

Our results clearly show that water in the microporous channels plays a crucial role in the observed electrochemical properties of the sitinakite electrodes. It remains possible that through judicious and careful structural engineering of the basic sitinakite framework some of its electrochemical deficiencies can be overcome. Initial attempts at niobium doping into the titanate sublattice do not appear to have yielded an improvement in performance. However, caution should be exercised in interpreting these results as the effects of drying on these “doped” variants is not necessarily to that of the parent compound. We plan to further investigate the effectiveness of doping with niobium and other transition metals.

Acknowledgment. The authors acknowledge Dr. P. Southon for his assistance in the preparation of some of the materials studied. The authors wish to acknowledge the Australian Research Council for their support of this project through Grant DP0346183. N.A.M. acknowledges support through an Australian Postgraduate Award.

CM0523337